

Received October 22, 2020, accepted October 28, 2020, date of publication November 3, 2020, date of current version November 13, 2020.

Digital Object Identifier 10.1109/ACCESS.2020.3035549

Multi-Step Segmentation Algorithm for Quantitative Magnetic Resonance Imaging T2 Mapping of Ruptured Achilles Tendons

PIOTR A. REGULSKI^{1,2}, (Member, IEEE), AND JAKUB ZIELIŃSKI³

¹Center of Digital Science and Technology, Cardinal Stefan Wyszyński University in Warsaw, 01-815 Warsaw, Poland

²Department of Dental and Maxillofacial Radiology, Medical University of Warsaw, 02-091 Warsaw, Poland

³Interdisciplinary Centre for Mathematical and Computational Modeling, University of Warsaw, 00-927 Warsaw, Poland

Corresponding author: Piotr A. Regulski (pregulski@interia.pl)

This work was supported by the National Centre for Research and Development (Poland) within the STRATEGMED Programme under Grant STRATEGMED1/233224/10/NCBR/2014.

ABSTRACT Diagnosis and treatment monitoring of Achilles tendon ruptures (ATRs) are supported by medical imaging, in particular by magnetic resonance imaging (MRI) for tendon volume and healing assessment. Therefore, we propose an automatic, multi-step segmentation algorithm for quantitative MRI T2 mapping of ATRs. Seventy retrospective post-trauma, post-surgery and follow-up studies were included in this research. The automatic segmentation algorithm for the inhomogeneous, noisy Achilles tendon region consisted of a multi-step anisotropic denoising, T2 map reconstruction with a weighted log-linear regression, thresholding with T2 time parameters, region growing and morphological closing. The automatic segmentation results were compared with those from manual contour tracing (MCT) performed by two radiologists. The Intersection over Union (IoU), specificity, sensitivity, F1-score, Yasnoff's normalized distance (YND), and type I and II errors were used to assess the segmentation accuracy. The segmentation methods were also compared with a Bland-Altman plot of the volumes of the segmented regions, with mean differences, correlation coefficients and 95% confidence intervals. The mean specificity and sensitivity values were high, $99.8 \pm 0.1\%$ and $85.9 \pm 8.7\%$, respectively, with corresponding type I and II errors of $0.2 \pm 0.1\%$ and $14.1 \pm 8.7\%$. The IoU, F1-score and YND were $71.0 \pm 9.2\%$, $82.7 \pm 6.3\%$ and $0.007 \pm 0.007\%$, respectively. The tendon volumes obtained by manual and automatic segmentation were strongly positively correlated ($R^2 = 0.85$), and the Bland-Altman plot depicted good comparability. The average difference was -28 voxels (95% confidence interval: -2726 to 2782 voxels). For ATRs, our method is reliable, with a strong positive correlation with MCT and a very high specificity.


INDEX TERMS Achilles tendon, image segmentation, magnetic resonance imaging, quantitative MRI, T2 mapping.

I. INTRODUCTION

The incidence of Achilles tendon ruptures (ATRs) or injuries has increased over the last few decades and is approximately 7-22 cases per 100,000 people in the general population [1]–[5]. ATRs are associated with both recreational activity and professional sport as well as increased workload [6]. The post-ruptured histochemical changes in the collagen fibres are reflected clinically only to a certain extent [7]. Therefore, diagnosis is supported by medical imaging. Magnetic resonance imaging (MRI) and ultrasound are commonly used for diagnosis and during the recovery process. In contrast to

ultrasound, MRI is regarded as more sensitive in discriminating pathology [8].

Most MRI sequences allow the qualitative evaluation of ongoing processes [9]. ATR images differ between sequences, patients and post-rupture or post-surgery times [10], [11]. Major changes occur mainly during the first half year after trauma and are caused by variations in the tissue water level and collagen fibril orientation during the regeneration process. The shape of the Achilles tendon depends on the distance from the rupture, on the associated oedema and even on the assessed level (distance between the rupture and the calcaneal enthesis) [12]. Heterogeneity in the size, brightness levels and fibre arrangements on MRI slices hinder the diagnosis and segmentation process (Fig. 1).

The associate editor coordinating the review of this manuscript and approving it for publication was Juan Wang .

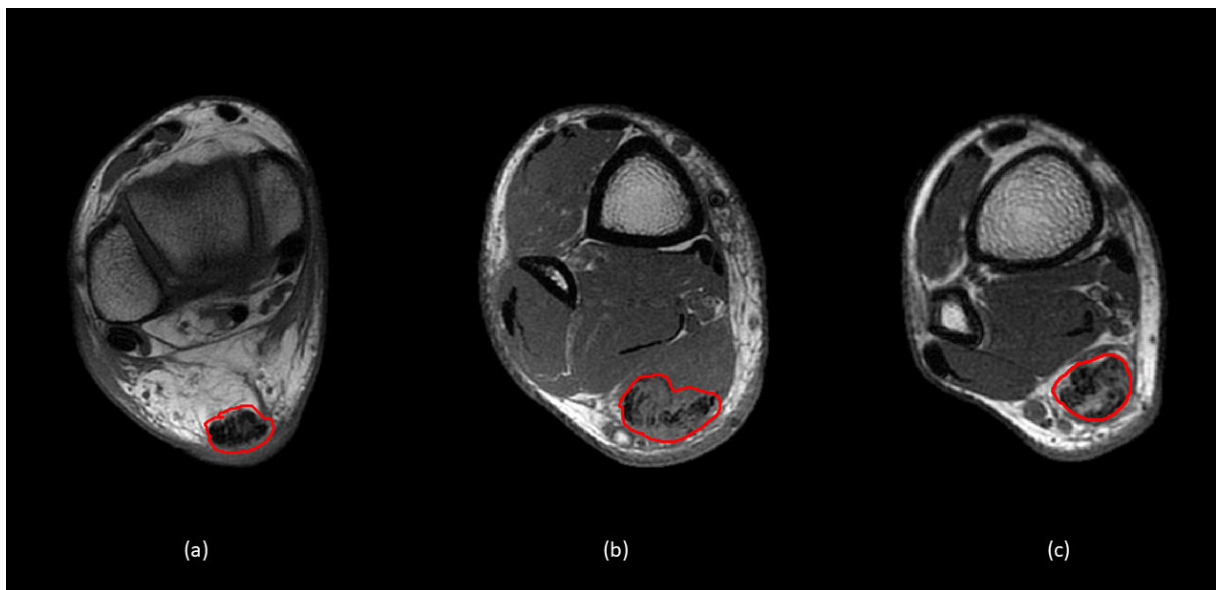


FIGURE 1. Manual segmentation of an ATR performed by a radiologist. Automatic segmentation is complicated due to variability in the shape, texture and intensity of the signal of the Achilles tendon. a) The internal structure of the Achilles tendon is hypointense (darker) and quite regular, with brighter fibrous scar tissue that divides the tendon area and makes the segmentation process more complex. b) Enlarged postoperative tendon area with non-homogeneous internal structure (hypo- and isointense regions). The isointense regions have similar density as surrounding anatomical structures. Therefore, a preprocessing step is necessary to depict the borderlines between the Achilles tendon and surrounding tissues. c) The post-ruptured, postoperative Achilles tendon area consists of hypo-, iso-, and hyperintense regions. The completely heterogeneous areas require processing in order to obtain homogeneous areas that can be segmented.

The variability in the tendon volume is one of the key factors assessed to evaluate its degeneration, and tendon texture analysis may be used to assess the healing process [13], [14]. Therefore, segmentation of the ruptured Achilles tendon is not a trivial task. To the best of our knowledge, segmentations or volume assessments of ATR are performed manually on MRI by contour tracing [15], [16]. This method is very time consuming and depends on the radiologist's experience. There are only a few manuscripts on automatic segmentation in healthy patients or patients with minor tendinopathy [17]–[19]. None of these studies used an automatic identification method on ruptured Achilles tendons.

The aim of this study is to present and evaluate a multi-step segmentation method for quantitative magnetic resonance images for ruptured Achilles tendons.

A quantitative T2-weighted sequence consists of several T2-weighted acquisitions obtained with different echo times and a map of the T2 relaxation times calculated for each image voxel (called a T2 map). The main advantage of a T2 maps is its superiority to other qualitative weighted MRI sequences due to its potential for providing quantitative and a more comprehensive characterization of tissues. Moreover, the assessment of T2 maps is commonly used during the diagnosis of ATRs [20].

II. MATERIAL

Seventy retrospective post-trauma, post-surgery and follow-up MRI studies of ATR patients were included in this research. A 1.5-T MRI unit (Signa HDxt, GE Medical Systems, Waukesha, USA) was used. For T2 time measurements, the fast multi-spin echo sequence was used. The T2 map imaging parameters were as follows: repetition

time = 1200 ms, eight echo times = {9, 18, ..., 72 ms}, field of view = $150 \times 150 \text{ mm}^2$, matrix = 512×512 voxels, slice resolution = $0.29 \times 0.29 \text{ mm}^2$, slice thickness = 3.5 mm, spacing between slices = 4.2 mm, 10 slices, and average acquisition time = 8:17 (min:sec). Each slice of a volume (10 slices in total) consists of images of eight different echo times. Therefore, a slice is represented by eight images, and segmentation of the slice is performed by using these images.

III. METHODS

The invention of the automated Achilles tendon segmentation algorithm was a multitask process due to the large inhomogeneity of tendon tissues and consisted of 1. a multi-step anisotropic denoiser (MSAD), 2. a weighted log-linear regression (WLLR) method for reconstructing mono-exponential T2 maps, 3. thresholding with the T2 time parameter, 4. region growing from a given seed point and 5. a morphological closing operation (Fig. 2). Automatic segmentation was compared with MCT performed by a radiologist. Segmentation quality measurements were introduced to assess the segmentation accuracy. Automatic segmentation and measurements were performed on the VisNow-Plugin-Medical library – a Java plugin for the open-source VisNow platform that allows medical analysis and visualization. The platform is available at <https://gitlab.com/cnt-uksw/visualization/VisNow> [21].

A. MULTI-STEP ANISOTROPIC DENOISER (MSAD)

The MSAD was used to decrease the high noise level of the obtained T2-weighted acquisitions. The low signal-to-noise ratio (SNR) of those acquisitions is considered a cause of distortions during the calculation of the T2 maps. The MSAD algorithm is used for noise reduction while preserving the

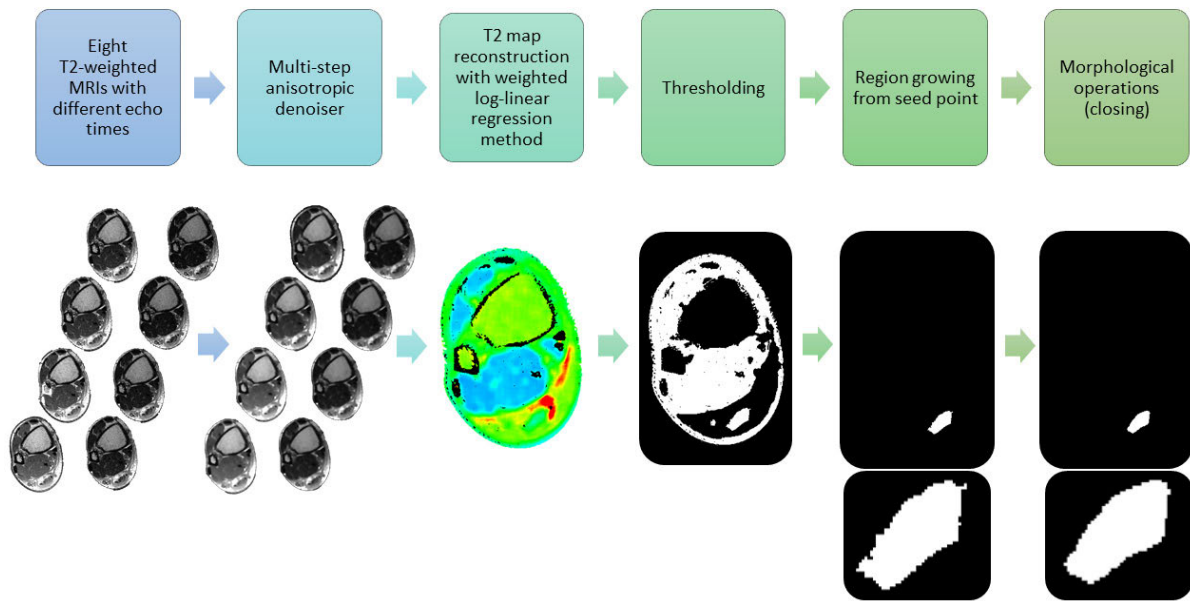


FIGURE 2. Subsequent steps of automated segmentation for ruptured Achilles tendons shown on a single slice obtained from a three-dimensional dataset (10 slices of eight T2-weighted sequences).

edges of uniform areas in the image in accordance with their local characteristics. The MSAD averages voxels with the use of weighted Gaussian smoothing and consists of two main steps. First, the standard Gaussian filter is calculated as the initial anisotropy field (w). Second, the weighted average is calculated from the local adaptive kernel given as the product of w and the correcting factor $\exp(-(w(p)-w(q))^2)$, where p is a centre and q is a neighbouring voxel within the kernel's radius. The kernel's radius is selected to neither cause the loss of small details nor to leave a significant noise level. The detailed description of MSAD was given by Regulski *et al.* in [22]. The customizable parameters in the MSAD algorithm were the kernel radius and standard deviation of the weighted Gaussian distribution (SDWGD). For segmentation preprocessing, the trial of 3 studies was chosen and assessed according to the highest values of IoU, specificity, and sensitivity. A kernel radius of 6 voxels and an SDWGD of 400 units proved to have the highest values of the above-mentioned measures and were chosen for further segmentation steps for the whole sample. The MSAD was performed for each slice separately due to the large spacing between slices. The two-dimensional MSAD was more efficient in time than the three-dimensional one. Furthermore, the 2D MSAD was chosen in order to exclude the heterogeneity artefacts associated with interpolation.

B. WEIGHTED LOG-LINEAR REGRESSION (WLLR) METHOD

There are several approaches to computing T2 maps [23]–[26]. Generally, the mono-exponential approximation of the model function for the $Y(t)$ signal of T2-weighted acquisitions is given by:

$$Y(t) = A \cdot \exp(-t/T) + N(t), \tag{1}$$

where t is the echo time, T is the relaxation time, A is the amplitude of the signal, and $N(t)$ is the noise level.

In this research, the mono-exponential weighted method is chosen due to its smoothing effect, which significantly simplifies the segmentation process [20]. Therefore, the mono-exponential approximation of the weighted model function for the $Y(t)$ signal is:

$$Y(t) = A \cdot \exp(-t/T) \cdot W(t) + N(t), \tag{2}$$

where $W(t)$ is the weights. The weights ($W(t)$) are introduced to reduce the role of noise in T2 map reconstruction. The weights are calculated within a window of a given radius (r) of one T2-weighted acquisition. The window slides through all the voxels of the image. The differences between the window centre (v_c) and neighbouring voxels (v_n) are calculated. If the difference is more than two standard deviations of all the voxels within the window, then v_n is rejected to avoid overestimate the noise within windows containing two or more regions of considerably different signals. The variance is calculated from the $m(t)$ -remaining voxels and is intended to be a local noise measure within the window. The weights are given by:

$$W(t) = \frac{1}{\frac{1}{m(t)} \cdot \sum_{i=1}^{m(t)} \sigma_i(t)^2} \tag{3}$$

where $m(t)$ is number of voxels left within window and $\sigma_i(t)^2$ is the variance in the $m(t)$ - remaining voxels.

For segmentation purposes, the weights are calculated with a large radius. The higher the radius, the more blurred the image is, and the simpler the segmentation is. However, an excessive increase in the radius blurs the boundaries between neighbouring regions. On the basis of experimental data, we have chosen $r = 6$ to be the best choice to fulfil the segmentation purposes.

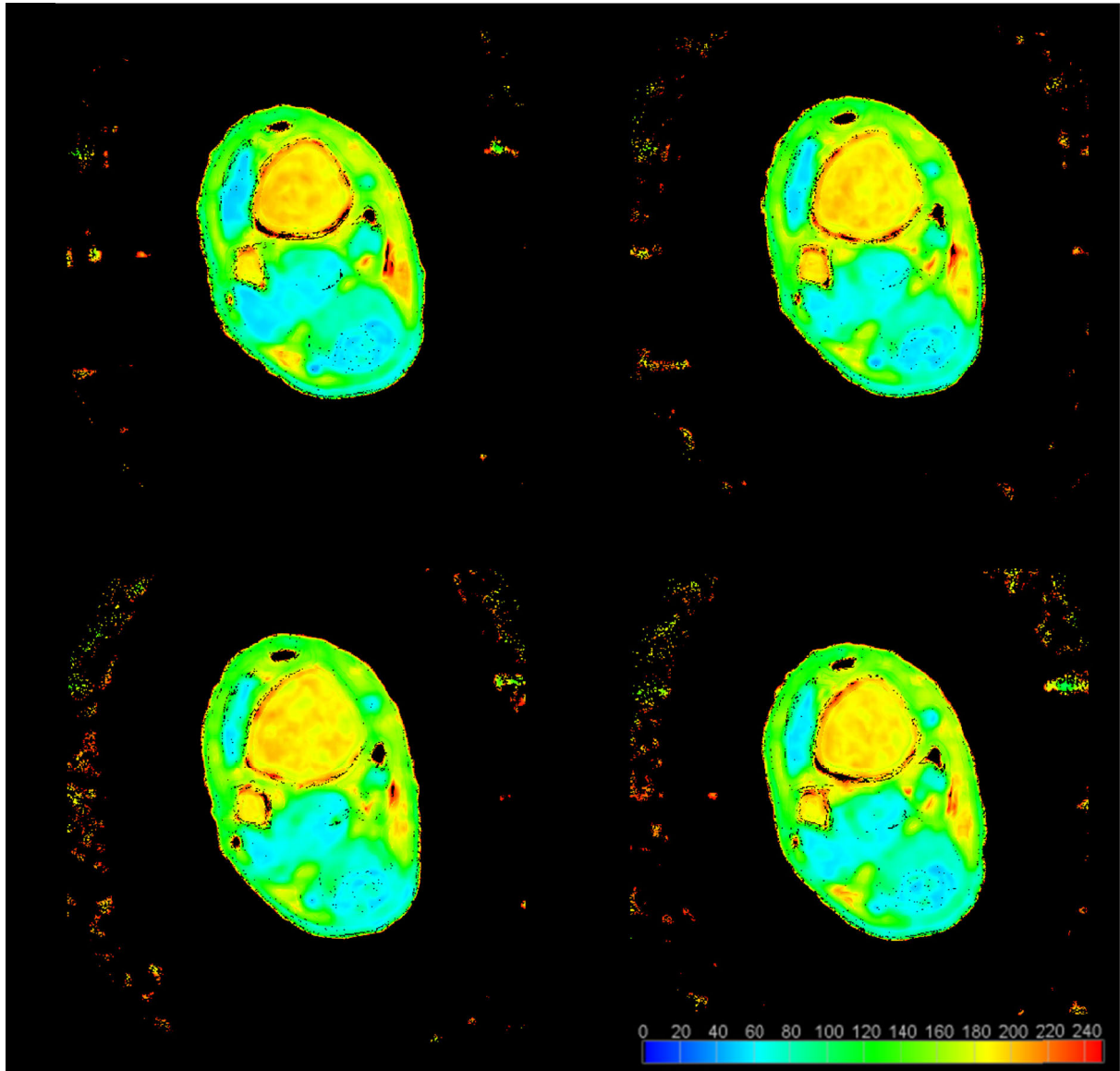


FIGURE 3. Four slices of a T2 map after WLLR reconstruction with a radius of 6.

In this research, the acquired spin echo images were highly affected by noise. The mean SNR was approximately 1.38. The low-SNR images may cause some distortions in the calculation of the T2 times. However, Gudbjartsson and Patz indicated that the MRI noise signal follows a Rician distribution. The Rician probability density function of the noise follows a Rayleigh distribution for a low-intensity signal (low SNR). Therefore, we can assume that low-signal Rayleigh noise satisfies the condition of a multiplicative noise distribution. The additive noise becomes multiplicative. The noise level ($N(t)$) can be incorporated into weights to reduce the number of approximated parameters [27]:

$$Y(t) = A \cdot \exp(-t/T) \cdot W_N(t), \quad (4)$$

where $W_N(t) = W(t) \bullet N(t)$ indicates the weight and the noise level.

Then, the WLLR method was applied. We estimated the relaxation time for each pixel of the T2 map. Consequently, the approximation function is given by:

$$y(t) = \alpha + \beta \cdot t + \omega(t), \quad (5)$$

where $y(t) = \ln(Y(t))$, $\alpha = \ln(A)$, and $\omega(t) = \ln(W_N(t))$.

An example of the obtained T2 map is presented in Fig. 3.

C. THRESHOLDING OF THE T2 MAPS

Thresholding of the T2 maps allowed the classification of the leg tissues into two groups: inside and outside a given threshold range. The upper threshold value was set to 90 ms, which corresponded to the average supremum the T2 time in the ruptured Achilles tendon area on MRIs taken immediately after trauma and surgery. During the recovery process, the T2 time decreases, therefore, for the follow-up studies, the upper threshold value was set to 70 ms. The lower

threshold was set to 1 ms to eliminate noise remaining in the air surrounding the patient's leg.

D. REGION GROWING

Classification with the use of the previous step divided the T2 map image into several regions containing T2 values from the threshold range. These regions were recognized as foreground, and a further segmentation process was conducted on them. The rest of the voxels were classified as background and considered unsuitable for the analysis. On most of the slices, the Achilles tendon region was connected to a few foreground regions. To single out the Achilles tendon area from all the other separate regions, the seed region growing algorithm was used [28]. We expected the Achilles tendon area to be in the same relative location in the lower limb in most cases and its centre-point to be located approximately at the same distance from the posterior outline of the leg (which was classified as foreground during thresholding) and close to the midline of the MRI slice. Therefore, the centre-point was estimated to be in the same relative position independent of the image. To overcome the errors related to image magnification, we used the normalized coordinates to estimate the centre-point. In the antero-posterior direction, the most posteriorly located foreground voxel was interpreted as 0 and the most anteriorly located voxel as 1. Additionally, in the medio-lateral direction, the rightmost voxel was interpreted as 0 and leftmost voxel as 1. The centre-point was estimated to be 0.16 and 0.50 in the antero-posterior and the medio-lateral directions, respectively.

The estimated foreground regions on one central slice were morphologically eroded (with a 12-voxel-radius kernel) due to overlap, and the centroid of the region located closest to the centre-point (the expected location of the Achilles tendon) was set as the initial seed point: therefore, the initial seed point was set automatically. The coordinates of the seed point were projected to other slices. Manual adjustment of seed points was also possible on each slice. The region growing algorithm was performed once per slice. The classification of voxels as Achilles tendon was provided with the ordering attribute. The ordering attribute was defined as the difference between the analysed voxel and the mean of the previously segmented voxels (within the Achilles tendon). The stopping criterion was obtained when the minimal ordering attribute of all neighbouring voxels was higher than the standard deviation of the segmented region voxels. A subsequent morphological closing operation was used to close gaps within a segmented mask (performed for each slice with a 10-voxel-radius kernel).

E. SEGMENTATIONS QUALITY MEASURE AND STATISTICS

The automatically segmented Achilles tendons were compared with manual contour tracing (MCT) performed by the two experienced radiologists (18 years and 9 years of experience in radiology, respectively) who traced the boundaries on 10 transverse slices in each study. The manual segmentation was possible to perform by taking into consideration the anatomy of the tendon and the surrounding structures.

The Achilles tendon was covered with the fascia, and posteriorly with the skin. Anteriorly, medially and laterally, the tendon was adjacent to the areolar, adipose or swollen tissue, which could be differentiated from the tendon on the T2-weighted images. OsiriX (Bernex, Switzerland) was applied for MCT [29]. The tendon was delineated with the "closed polygon" tool. Small inaccuracies were eliminated with the "repulser" tool.

We used several common segmentation quality measures, namely, the mean Intersection over Union (IoU), specificity, sensitivity (mean accuracy), F1-score, type I and II errors, and Yasnoff's normalized discrepancy distance, to compare our automatic segmentation algorithm with MCT [30]. Descriptive statistics were calculated for all the measures. The inter-observer reliability was assessed with the intra-class correlation coefficient (ICC) based on a mean-rating, 2-way mixed-effects model and calculated based on the quality measures.

The automatic and averaged MCT (from two radiologists) segmentation methods were also compared with Bland-Altman plots of the volumes (numbers of voxels) of the segmented regions, mean differences, correlation coefficients (R^2) and 95% confidence intervals. In the similar manner, the correlation coefficients and 95% confidence intervals between manually traced volumes obtained by both radiologists were calculated. The statistical analysis was performed using Statistica (Tibco, Palo Alto, USA) and Excel (Microsoft, Redmond, USA).

IV. RESULTS

For the comparison of the MCT and automatic segmentation methods, 70 ruptured Achilles tendons were analysed (Fig. 4). The mean IoU, specificity, sensitivity, F1-score and errors were calculated according to the true positive, false positive, true negative and false negative voxels, which are the correctly identified, incorrectly identified, correctly rejected and incorrectly rejected voxels, respectively.

The specificity was very high (greater than 99%), and the type I error was low (less than 0.5%); therefore, incorrectly rejected voxels were in the minority. The values of the sensitivity (85.9%) and type II error (14.1%) suggest that the majority of voxels were classified correctly. The spatial information of the missegmented voxels was taken into account during the assessment of Yasnoff's distance (approximately 0.007%), which was calculated as the average distance between the missegmented voxels and the nearest ones that belong to the manually segmented region and was normalized to the image dimensions. The average values and standard deviations of all measurements (from both radiologists) are shown in table 1. The inter-rater reliability was excellent in terms of IoU, F1-score, specificity and sensitivity (ICC > 90%). Good reliability was obtained for Yasnoff's distance and type I and II errors (ICC > 75%, Table 1).

The comparison of the ATR volumes (numbers of voxels) obtained with the averaged MCT and automatic segmentation methods showed a strong positive correlation

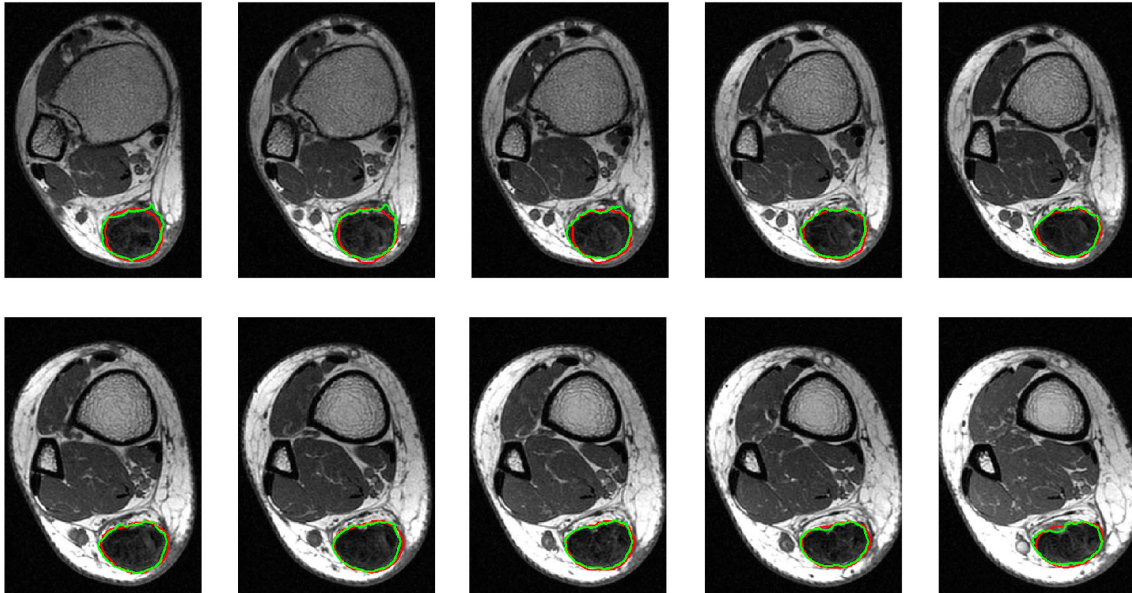


FIGURE 4. Typical example of the segmentation results. The automatically segmented region is marked in green, and the manual segmentation performed by the radiologist is marked in red.

TABLE 1. Average values, standard deviations and inter-observer reliability of the comparative measurements from manual and automatic segmentation.

Measure	Average \pm standard deviation	Inter-observer reliability
Intersection over Union	0.710 \pm 0.092	97.4%
Specificity	0.998 \pm 0.001	95.5%
Sensitivity	0.859 \pm 0.087	96.6%
F1-score	0.827 \pm 0.063	99.7%
Type I error	0.002 \pm 0.001	89.1%
Type II error	0.141 \pm 0.087	89.2%
Yasnoff's distance	7.482E-05 \pm 7.012E-05	89.7%

($R^2 = 0.85$, Fig. 5). The Bland-Altman plot depicted good comparability between the two methods. The average difference was -28 voxels (-8.2 mm^3), and the 95% confidence interval was -2726 to 2782 voxels (-802.4 to 818.9 mm^3). Therefore, the algorithm showed a slight tendency towards under-segmentation. Fig. 6. The strong positive correlation was also obtained between ATR volumes manually traced by two radiologists ($R^2 = 0.95$). The 95% confidence interval was $-2,068$ to $2,084$ voxels (-608.9 to 613 mm^3).

The total computational time of the whole process of segmentation was 68.461 ± 0.620 s on a computer station with an 8-core Intel Xeon Processor E5-2687 W. The time consisted of MSAD, WLLR, thresholding, region growing and morphological operation times: 9.267 ± 0.183 s, 57.959 ± 0.424 s, 0.008 ± 0.002 s, 1.520 ± 0.776 s, and 0.148 ± 0.620 s, respectively.

V. DISCUSSION

We would like to emphasize that, to the best of our knowledge, this is the first study that presents an automatic segmentation algorithm for ruptured Achilles tendons. We conducted a systematic electronic search in October 2019 with the key words (Achilles tendon rupture, automatic segmentation and magnetic resonance imaging) in

Embase, Medline and Web of Science without obtaining any results. Achilles tendon volume variability is a widely recognized factor in the healing process. Therefore, we relaxed our search criteria to find methods that assess volume changes in ruptured Achilles tendons (key words: Achilles tendon rupture, volume, length, MRI). Twenty-nine of the 45 found articles were rejected due to either the usage of different diagnostic modalities or the assessment of changes in Achilles-tendon-neighbouring anatomical structures after its rupture. In the remaining 16 articles, the assessment was performed either by analysis of variability of ATR linear measurements and manually acquired tendon volumes or by clinical scores [13], [31]–[36].

We also searched for segmentation methods for the Achilles tendon volume with different tendinopathies (without specifying a rupture; key words: Achilles tendon, volume, length, MRI). Only five out of the 25 located articles concerned automatic segmentation [17]–[19], [37], [38]. We would like to emphasize that we were searching not only for segmentations of Achilles tendon ruptures but also for segmentations and volume measures of healthy tendons and those with tendinopathy. In contrast to ATR segmentation, tendinopathy segmentation was simpler due to the homogeneous texture of the tendon. Large differences in the MRI

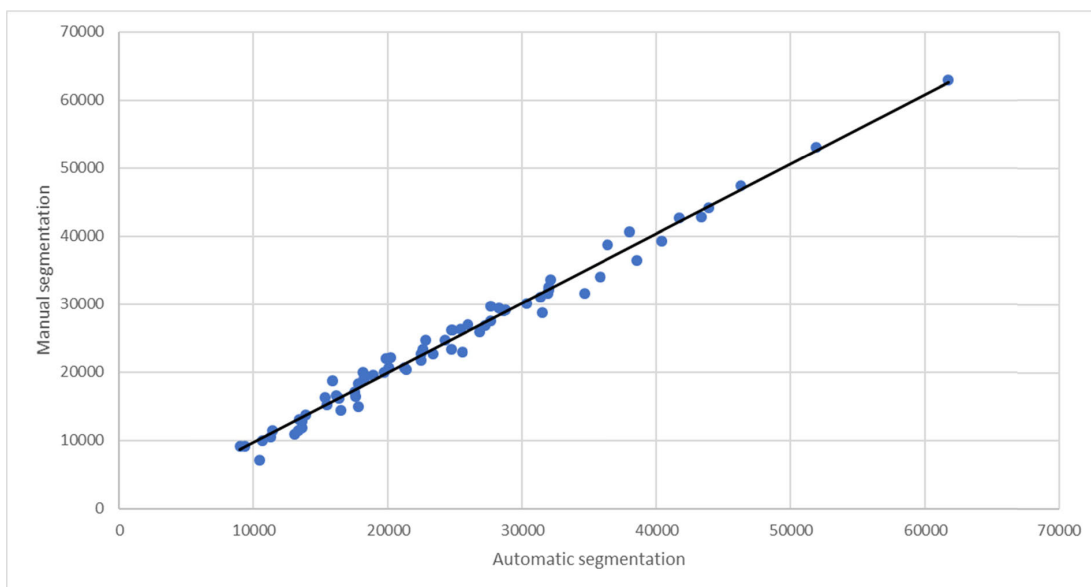


FIGURE 5. Correlation plot: the tendon volume calculated from manual segmentation vs. the tendon volume calculated from automatic segmentation, measured in voxels ($R^2 = 0.85$).

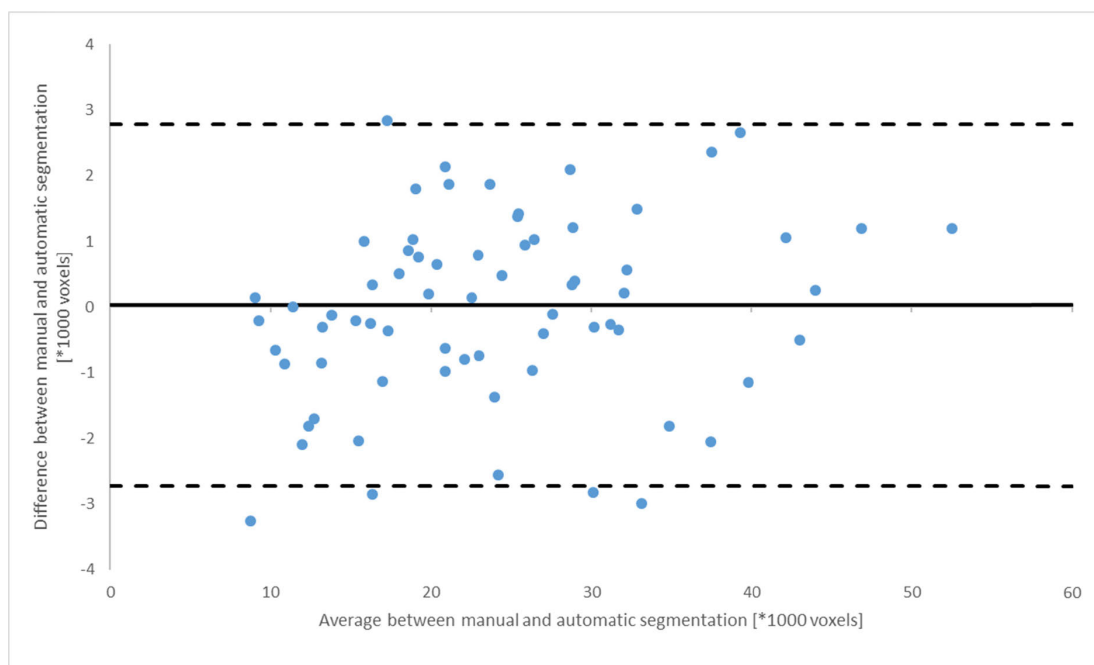


FIGURE 6. Bland-Altman plot of the manually and automatically segmented tendon volumes. The mean difference is marked with a solid line, and the 95% confidence intervals are indicated with dashed lines.

signals were not found in the tendon area, especially due to the short T2 and T2* relaxation times for the Achilles tendon. The segmentation task was also simpler due to the lack of time-related volume changes during the rupture healing process. Therefore, the obtained correlation coefficients and reliability in manually and automatically traced tendinopathy of non-ruptured Achilles tendons in different studies were high and ranged from 0.88 to 0.99.

Shalabi *et al.* [37] developed a 3D seed growing algorithm that relies on T1-weighted and proton density (PD)-weighted signal levels and their gradients. The seed point was selected manually. The inclusion criteria of the neigh-

boring voxels were checked to handle leakage problems. Automatically segmented tendons were compared with tendons manually segmented by two independent radiologists. The obtained reliabilities depending on the coefficient of variation were 0.881 and 0.979 for the T1- and PD-weighted signals, respectively. Gärdin *et al.* [19], [38] presented a similar seed growing algorithm on five MR sequences; however, this research did not contain a comparative analysis with a manually segmented ground-truth sequence.

Syha *et al.* [17], [18] presented a contour detection/segmentation algorithm of the Achilles tendon of healthy volunteers and tendinopathy patients. The algorithm con-

sisted of three main steps: 1. tracking the outer contour of the leg, 2. subsequent seed growing of the tendon area and morphology closing, and 3. tracking the boundary of the Achilles tendon with an active contour model. Manual correction was performed in cases of missegmentation. The correlation coefficient for the manual vs. automatic segmentation results was 0.99 in the group of healthy volunteers. The obtained sensitivity and specificity values within the group of tendinopathy patients ranged between 0.768-0.962 and 0.731-0.808, respectively, and depended on the distance from proximal to the cranial border of the calcaneal bone.

In our research, the mean sensitivity value of the ATR segmentation was higher than that of Syha *et al.*'s [17], [18] method for the proximal and distal parts and lower for the medial part of the tendon. The specificity for our method was higher than that for Syha *et al.*'s [17], [18] method in all cases, and the other statistics were not comparable. Manual correction was not performed.

The mean IoU, sensitivity, F1-score and type II error values, described within this manuscript, were characterized by high standard deviations. Therefore, there were some studies in which automatic segmentation gave worse results, which corresponded with our observations that in late follow-up studies (3-6 months postoperation) the presented algorithm was not ideal.

The longer the time after the surgery, the more homogeneous the tendon's image is and the more similar the tendon is to the surrounding tissues. The weights that were used in the WLLR reconstruction method excessively blurred the image. The boundaries between the Achilles tendon and its surrounding structures were not distinguishable. In those cases, better segmentation results should be expected with the use of simple region growing or active contour algorithms.

Our algorithm consisted of simple thresholding and region growing with morphological closing operation. The lack of a sophisticated segmentation algorithm was made possible due to advanced preprocessing steps such as MSAD and WLLR. This made the total algorithm simpler and potentially usable in other applications. The described method can be successfully used for the segmentation of other anatomical structures. We obtained promising results from the method described in this manuscript for segmenting the displaced disc for patients with temporomandibular joint disorders on T2 mapping sequences. However, further studies are required.

Automatic segmentation of a ruptured Achilles tendon improves the automatic assessment of its healing process. The future directions and continuation of our research concern the assessment of the stage of the healing process of the tendon after rupture. In the clinical evaluation of the healing process, it is extremely important to indicate the time when the tendon can start loading. The combination of the segmentation algorithm with feature analysis provides promising results. In our study, the patients underwent T2 mapping, and other sequences of MRI were taken after trauma, one, three, six, nine, twelve and twenty weeks after and as a follow-up to

surgery (up to 26 weeks after surgery). In the segmented region of the Achilles tendon with the algorithm presented in this manuscript, the T2 times are calculated, and the other tendon features such as size, shape, and texture are extracted. A variability assessment of segmented tendon features and their decomposition allows an indication of the stage of healing of the tendon. The combination of the segmentation algorithm with feature analysis highlights the need to advance to the next stage of treatment and rehabilitation. Further studies are required, however, to analyse the healing process [39].

VI. CONCLUSION

In conclusion, this is the first study that presents an automatic segmentation algorithm for ruptured Achilles tendons. The method utilizes a multi-step anisotropic denoiser, weighted log-linear regression reconstruction, region growing and thresholding algorithms. It proved to be reliable for quantitative MRIs. Compared to MCTs performed by the two experienced radiologists, it showed a strong positive correlation and very high specificity. Taking into consideration the other studies evaluating the automatic segmentation algorithms of simpler cases – that is, the non-ruptured Achilles tendons with tendinopathies – the sensitivity and specificity are the highest in our method, proving its superiority. The multi-step segmentation method of ATR provides a first step for complex algorithms analysing the healing process of the Achilles tendon.

ACKNOWLEDGMENT

The authors would like to acknowledge Dr. Beata Ciszowska-Lyson for performing MCT of the Achilles tendons and the National Centre for Research and Development (Poland) for co-funding this research as a part of the "Novel Scaffold-based Tissue Engineering Approaches to Healing and Regeneration of Tendons and Ligaments (START)" project within the STRATEGMED programme (STRATEGMED1/233224/10/NCBR/2014).

REFERENCES

- [1] S. Houshian, T. Tscherning, and P. Riegels-Nielsen, "The epidemiology of Achilles tendon rupture in a Danish county," *Injury*, vol. 29, no. 9, pp. 651–654, Nov. 1998, doi: [10.1016/S0020-1383\(98\)00147-8](https://doi.org/10.1016/S0020-1383(98)00147-8).
- [2] I. Lantto, J. Heikkinen, T. Flinkkilä, P. Ohtonen, and J. Leppilähti, "Epidemiology of achilles tendon ruptures: Increasing incidence over a 33-year period," *Scandin. J. Med. Sci. Sports*, vol. 25, no. 1, pp. e133–e138, Feb. 2015, doi: [10.1111/sms.12253](https://doi.org/10.1111/sms.12253).
- [3] T. Nyyssönen, P. Lähje, and H. Kröger, "The increasing incidence and difference in sex distribution of achilles tendon rupture in finland in 1987–1999," *Scandin. J. Surgery*, vol. 97, no. 3, pp. 272–275, Sep. 2008, doi: [10.1177/145749690809700312](https://doi.org/10.1177/145749690809700312).
- [4] A. Ganestam, T. Kallemose, A. Troelsen, and K. W. Barford, "Increasing incidence of acute achilles tendon rupture and a noticeable decline in surgical treatment from 1994 to 2013. A nationwide registry study of 33,160 patients," *Knee Surgery, Sports Traumatology, Arthroscopy*, vol. 24, no. 12, pp. 3730–3737, Dec. 2016, doi: [10.1007/s00167-015-3544-5](https://doi.org/10.1007/s00167-015-3544-5).
- [5] D. W. White, J. C. Wenke, D. S. Mosely, S. B. Mountcastle, and C. J. Basamania, "Incidence of major tendon ruptures and anterior cruciate ligament tears in US army soldiers," *Amer. J. Sports Med.*, vol. 35, no. 8, pp. 1308–1314, Aug. 2007, doi: [10.1177/0363546507301256](https://doi.org/10.1177/0363546507301256).

- [6] A. Vadalá, "Functional evaluation of professional athletes treated with a mini-open technique for achilles tendon rupture," *Muscles, Ligaments Tendons J.*, vol. 15, pp. 177–181, Dec. 2014, doi: [10.11138/mltj/2014.4.2.177](https://doi.org/10.11138/mltj/2014.4.2.177).
- [7] V. Juras, S. Apprich, C. Pressl, S. Zbryn, P. Szomolanyi, S. Domayer, J. G. Hofstaetter, and S. Trattnig, "Histological correlation of 7T multi-parametric MRI performed in ex-vivo achilles tendon," *Eur. J. Radiol.*, vol. 82, no. 5, pp. 740–744, May 2013, doi: [10.1016/j.ejrad.2011.09.022](https://doi.org/10.1016/j.ejrad.2011.09.022).
- [8] B. Ciszowska-Lyson, U. Zdanowicz, A. Rosinska, M. Syrek, and R. Smigielski, "Establishing MR and ultrasound based model of a properly healing Achilles tendon allowing to properly determine the healing stage of the structure: Preliminary findings," in *Proc. Eur. Congr. Radiol.*, Vienna, Austria, Feb./Mar. 2018, Paper C-3209.
- [9] F. Hahn, P. Meyer, C. Maiwald, M. Zanetti, and P. Vienne, "Treatment of chronic achilles tendinopathy and ruptures with flexor hallucis tendon transfer: Clinical outcome and MRI findings," *Foot Ankle Int.*, vol. 29, no. 8, pp. 794–802, Aug. 2008, doi: [10.3113/FAI.2008.0794](https://doi.org/10.3113/FAI.2008.0794).
- [10] A. Fujikawa, Y. Kyoto, M. Kawaguchi, Y. Naoi, and Y. Ukegawa, "Achilles tendon after percutaneous surgical repair: Serial MRI observation of uncomplicated healing," *Amer. J. Roentgenol.*, vol. 189, no. 5, pp. 1169–1174, Nov. 2007, doi: [10.2214/ajr.07.2260](https://doi.org/10.2214/ajr.07.2260).
- [11] N. Maffulli, A. P. Thorpe, and F. W. Smith, "Magnetic resonance imaging after operative repair of achilles tendon rupture," *Scandin. J. Med. Sci. Sports*, vol. 11, no. 3, pp. 156–162, Jun. 2001, doi: [10.1046/j.1524-4725.2001.110305_1.x](https://doi.org/10.1046/j.1524-4725.2001.110305_1.x).
- [12] H. Weinreb Jeffrey, "Tendon structure, disease, and imaging," *Muscle, Ligaments Tendons J.*, vol. 4, no. 1, pp. 66–73, Jan. 2014.
- [13] C. Rosso, P. Vavken, C. Polzer, D. M. Buckland, U. Studler, L. Weisskopf, M. Lottenbach, A. M. Müller, and V. Valderrabano, "Long-term outcomes of muscle volume and achilles tendon length after achilles tendon ruptures," *Knee Surgery, Sports Traumatol., Arthroscopy*, vol. 21, no. 6, pp. 1369–1377, Jun. 2013, doi: [10.1007/s00167-013-2407-1](https://doi.org/10.1007/s00167-013-2407-1).
- [14] U. Grosse, R. Syha, S. Partovi, D. Keßler, M. Bongers, F. Seith, K. Nikolaou, M. Robbin, F. Schick, and F. Springer, "Intradial fluctuations of off-resonance saturation effects in healthy human achilles tendons assessed with a 3D ultrashort echo time MRI sequence at 3 tesla," *RöFo - Fortschritte auf dem Gebiet der Röntgenstrahlen und der bildgebenden Verfahren*, vol. 187, no. 11, pp. 1003–1010, Jun. 2015, doi: [10.1055/s-0035-1553187](https://doi.org/10.1055/s-0035-1553187).
- [15] A. Shalabi, M. Kristoffersen-Wiberg, P. Aspelin, and T. Movin, "MR EVALUATION OF CHRONIC ACHILLES TENDINOSIS. A longitudinal study of 15 patients preoperatively and two years postoperatively," *Acta Radiologica*, vol. 42, no. 3, pp. 269–276, May 2001, doi: [10.1034/j.1600-0455.2001.042003269.x](https://doi.org/10.1034/j.1600-0455.2001.042003269.x).
- [16] L. Nuri, S. J. Obst, R. Newsham-West, and R. S. Barrett, "Three-dimensional morphology and volume of the free achilles tendon at rest and under load in people with unilateral mid-portion achilles tendinopathy," *Experim. Physiol.*, vol. 103, no. 3, pp. 358–369, Mar. 2018, doi: [10.1113/ep086673](https://doi.org/10.1113/ep086673).
- [17] R. Syha, F. Springer, C. Wrslin, I. Ipach, D. Ketelsen, G. Grözinger, M. Notohamiprodjo, K. Nikolaou, C. D. Claussen, F. Schick, and U. Grosse, "Tendinopathy of the achilles tendon: Volume assessed by automated contour detection in submillimeter isotropic 3-Dimensional magnetic resonance imaging data sets recorded at a field strength of 3 t," *J. Comput. Assist. Tomogr.*, vol. 39, no. 2, pp. 250–256, 2015, doi: [10.1097/rct.0000000000000203](https://doi.org/10.1097/rct.0000000000000203).
- [18] R. Syha, C. Wrslin, D. Ketelsen, P. Martirosian, U. Grosse, F. Schick, C. D. Claussen, and F. Springer, "Automated volumetric assessment of the achilles tendon (AVAT) using a 3D t2 weighted SPACE sequence at 3T in healthy and pathologic cases," *Eur. J. Radiol.*, vol. 81, no. 7, pp. 1612–1617, Jul. 2012, doi: [10.1016/j.ejrad.2011.04.016](https://doi.org/10.1016/j.ejrad.2011.04.016).
- [19] A. Gärdin, J. Bruno, T. Movin, M. Kristoffersen-Wiberg, and A. Shalabi, "Magnetic resonance signal, rather than tendon volume, correlates to pain and functional impairment in chronic achilles tendinopathy," *Acta Radiologica*, vol. 47, no. 7, pp. 718–724, Sep. 2006, doi: [10.1080/02841850600774035](https://doi.org/10.1080/02841850600774035).
- [20] P. A. Regulski, J. Zieliński, B. A. Borucki, and K. S. Nowinski, "Comparison of noise reducing T2-map reconstruction methods in MRI imaging of Achilles tendon," *Int. J. Comput. Assist. Radiol. Surg.*, vol. 12, pp. 15–16, Jun. 2017.
- [21] K. S. Nowinski and B. Borucki, "VisNow - a modular, extensible visual analysis platform," in *Proc. 22nd Int. Conf. Central Eur. Comput. Graph. Vis. Comput. Vis.*, vol. 2014, pp. 73–76.
- [22] P. Regulski, J. Zieliński, B. Borucki, and K. Nowiski, "Assessment of anisotropic denoiser enhanced cone beam CT for patient dose reduction," *Int. J. Comput. Assist. Radiol. Surg.*, vol. 10, pp. 295–296, Jun. 2015.
- [23] H. Adriaensens, M. Musse, S. Quellec, A. Vignaud, M. Cambert, and F. Mariette, "MSE-MRI sequence optimisation for measurement of bi- and tri-exponential t2 relaxation in a phantom and fruit," *Magn. Reson. Imag.*, vol. 31, no. 10, pp. 1677–1689, Dec. 2013, doi: [10.1016/j.mri.2013.02.004](https://doi.org/10.1016/j.mri.2013.02.004).
- [24] J. G. Raya, O. Dietrich, A. Hornig, J. Weber, M. F. Reiser, and C. Glaser, "T2 measurement in articular cartilage: Impact of the fitting method on accuracy and precision at low SNR," *Magn. Reson. Med.*, vol. 63, no. 1, pp. 181–193, Jan. 2010, doi: [10.1002/mrm.22178](https://doi.org/10.1002/mrm.22178).
- [25] M. Akçakaya, T. A. Basha, S. Weingärtner, S. Roujol, S. Berg, and R. Nezafat, "Improved quantitative myocardial T2 mapping: Impact of the fitting model," *Magn. Reson. Med.*, vol. 74, no. 1, pp. 93–105, Jul. 2015, doi: [10.1002/mrm.25377](https://doi.org/10.1002/mrm.25377).
- [26] M. Björk, D. Zachariah, J. Kullberg, and P. Stoica, "A multicomponent T2 relaxometry algorithm for myelin water imaging of the brain," *Magn. Reson. Med.*, vol. 75, no. 1, pp. 390–402, Jan. 2016, doi: [10.1002/mrm.25583](https://doi.org/10.1002/mrm.25583).
- [27] H. Gudbjartsson and S. Patz, "The rician distribution of noisy mri data," *Magn. Reson. Med.*, vol. 34, no. 6, pp. 910–914, Dec. 1995, doi: [10.1002/mrm.1910340618](https://doi.org/10.1002/mrm.1910340618).
- [28] S.-Y. Wan and W. E. Higgins, "Symmetric region growing," *IEEE Trans. Image Process.*, vol. 12, no. 9, pp. 1007–1015, Sep. 2003, doi: [10.1109/TIP.2003.815258](https://doi.org/10.1109/TIP.2003.815258).
- [29] A. Rosset, L. Spadola, and O. Ratib, "OsiriX: An open-source software for navigating in multidimensional DICOM images," *J. Digit. Imag.*, vol. 17, no. 3, pp. 205–216, Sep. 2004, doi: [10.1007/s10278-004-1014-6](https://doi.org/10.1007/s10278-004-1014-6).
- [30] Y. J. Zhang, "A survey on evaluation methods for image segmentation," *Pattern Recognit.*, vol. 29, no. 8, pp. 1335–1346, 1996, doi: [10.1016/0031-3203\(95\)00169-7](https://doi.org/10.1016/0031-3203(95)00169-7).
- [31] J. Heikkinen, I. Lantto, T. Flinkkila, P. Siira, V. Laine, J. Niinimäki, P. Ohtonen, and J. Leppilähti, "Calf muscle atrophy and achilles tendon elongation after acute achilles tendon rupture," *Arthroscopy, J. Arthroscopic Rel. Surg.*, vol. 33, no. 10, pp. e129–e130, Oct. 2017, doi: [10.1016/j.arthro.2017.08.153](https://doi.org/10.1016/j.arthro.2017.08.153).
- [32] J. Heikkinen, I. Lantto, J. Piilonen, T. Flinkkilä, P. Ohtonen, P. Siira, V. Laine, J. Niinimäki, A. Pajala, and J. Leppilähti, "Tendon length, calf muscle atrophy, and strength deficit after acute achilles tendon rupture: Long-term follow-up of patients in a previous study," *J. Bone Joint Surg.-Amer. Volume*, vol. 99A, no. 18, pp. 1509–1515, Sep. 2017, doi: [10.2106/jbjs.16.01491](https://doi.org/10.2106/jbjs.16.01491).
- [33] J. Zhan, J. Fang, J. Zhang, W. Cheng, H. Lu, and J. Jing, "Effectiveness of modified suture technique in treatment of acute closed Achilles tendon rupture," *Zhongguo Xiu Fu Chong Jian Wai Ke Za Zhi*, vol. 31, no. 8, pp. 952–956, Aug. 2017, doi: [10.7507/1002-1892.201702090](https://doi.org/10.7507/1002-1892.201702090).
- [34] T. L. Miller and S. Shemery, "Insertional achilles tendon injuries in the athlete," *Oper. Techn. Sports Med.*, vol. 25, no. 2, pp. 87–98, Jun. 2017, doi: [10.1053/j.otsm.2017.03.006](https://doi.org/10.1053/j.otsm.2017.03.006).
- [35] T. Yasuda, H. Shima, K. Mori, M. Kizawa, and M. Neo, "Direct repair of chronic achilles tendon ruptures using scar tissue located between the tendon stumps," *J. Bone Joint Surg.*, vol. 98, no. 14, pp. 1168–1175, Jul. 2016, doi: [10.2106/jbjs.15.00865](https://doi.org/10.2106/jbjs.15.00865).
- [36] A. F. Sadek, E. H. Fouly, M. A. Laklok, and M. F. Amin, "Functional and MRI follow-up after reconstruction of chronic ruptures of the achilles tendon myerson type III using the triple-loop plantaris tendon wrapped with central turnover flap: A case series," *J. Orthopaedic Surg. Res.*, vol. 10, no. 1, p. 109, Jul. 2015, doi: [10.1186/s13018-015-0256-y](https://doi.org/10.1186/s13018-015-0256-y).
- [37] A. Shalabi, T. Movin, M. Kristoffersen-Wiberg, P. Aspelin, and L. Svensson, "Reliability in the assessment of tendon volume and intratendinous signal of the achilles tendon on MRI: A methodological description," *Knee Surg., Sports Traumatol., Arthroscopy*, vol. 13, no. 6, pp. 492–498, Sep. 2005, doi: [10.1007/s00167-004-0546-0](https://doi.org/10.1007/s00167-004-0546-0).
- [38] A. Gärdin, T. Movin, L. Svensson, and A. Shalabi, "The long-term clinical and MRI results following eccentric calf muscle training in chronic achilles tendinosis," *Skeletal Radiol.*, vol. 39, no. 5, pp. 435–442, May 2010, doi: [10.1007/s00256-009-0798-3](https://doi.org/10.1007/s00256-009-0798-3).

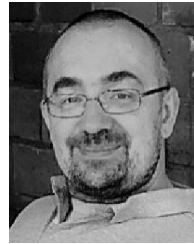
- [39] N. Kapinski, J. Zielinski, B. A. Borucki, T. Trzcinski, B. Ciszowska-Lyson, and K. S. Nowinski, "Estimating Achilles tendon healing progress with convolutional neural networks," in *Medical Image Computing and Computer Assisted Intervention*, A. F. Frangi, J. A. Schnabel, C. Davatzikos, C. Alberola-López, G. Fichtinger, Eds. Cham, Switzerland: Springer, 2018, pp. 949–957.



PIOTR A. REGULSKI (Member, IEEE) received the D.M.D. degree in medicine and dentistry from the Medical University of Warsaw, in 2010, the B.S. degree in electronic engineering from the Warsaw University of Technology, in 2011, and the Ph.D. degree in dentistry and informatics from the Medical University of Warsaw.

From 2012 to 2018, he was a Technical Assistant with the Interdisciplinary Centre for Mathematical and Computational Modeling, University of Warsaw. Since 2011, he has been a Research Assistant with the Dentomaxillofacial Radiology Department, Medical University of Warsaw, and since 2019, he has been an Assistant Professor with the Center of Digital Science and Technology, Cardinal Stefan Wyszyński University in Warsaw. His research interests include medical image processing, magnetic resonance, computer-aided diagnosis, and scientific visualization in medicine and dentistry.

Dr. Regulski is a Founding Member of the Association of Scientific Visualization (visnow.org) and an Associate Member of the International and European Academy of Dentomaxillofacial Radiology, the European Society of Radiology, IEEE Engineering in Medicine and Biology Society, and IEEE Computer Society Technical Committee on Pattern Analysis and Machine Intelligence.



JAKUB ZIELIŃSKI was born in Warsaw, Poland, in 1977. He received the M.S. degree in theoretical physics and the Ph.D. degree in physics from the University of Warsaw, in 2001 and 2006, respectively. From 2001 to 2018, he was a Senior Lecturer with the Department of Biophysics and Human Physiology, Warsaw Medical University.

Since 2013, he has been working with the Interdisciplinary Centre for Mathematical and Computational Modeling, University of Warsaw. He is a coauthor of one book and scientific articles. His research interests include medical imaging, quantum physics, and electrophysiology.

...